Lehtonen, V. J. *et al. Géotechnique* [http://dx.doi.org/10.1680/geot.14.P.100]

Full-scale embankment failure test under simulated train loading

V. J. LEHTONEN*, C. L. MEEHAN†, T. T. LÄNSIVAARA* and J. N. MANSIKKAMÄKI*

A full-scale embankment failure experiment was conducted in 2009 in Perniö, Finland. A small, extensively instrumented railway embankment on a soft clay foundation was brought to failure by loading over a period of 30 h. Instrumentation consisted of over 300 different measurement points, including 37 piezometers and nine automatically monitored inclinometer tubes. The relatively rapid loading simulated a heavy train coming to a standstill on the embankment. The primary purpose of the experiment was to gather field data of a failure caused by a rapidly applied load, with an emphasis on the pore pressure response in the clay foundation layer. The test was also used to assess the suitability of various instruments for real-time stability monitoring. The embankment failure was an asymmetric bearing capacity mechanism that is hypothesised to have been triggered by an undrained creep rupture. During the last 2 h of the experiment, pore pressure and displacements increased at an accelerating rate while the external load was kept constant. The time-dependency of the pore pressure and displacement responses was a key factor in the experiment. With regards to monitoring of similar in-service train embankments, proper placement of instruments according to predicted failure mechanisms was found to be important.

KEYWORDS: clays; creep; embankments; failure; full-scale tests; pore pressures

INTRODUCTION

For many projects around the world, assessment of geotechnical stability requires evaluation of the undrained capacity of clays. This capacity depends on many factors such as the effective stresses, stress and time history, the direction and rate of loading, and temperature (Leroueil & Marques, 1996). In ultimate limit state design, the undrained behaviour of a clay soil is often simplified by using a stress-independent constant value, that is, the undrained shear strength (s_u). In conventional design, the effect of stress and loading history is typically accounted for by determining s_u either in situ or at an appropriate stress level. The effects of loading rate are typically accounted for by performing undrained strength tests at a standardised shear rate, and in the case of the field vane, the measured values are then corrected using clay index properties (e.g. Bjerrum, 1973; Helenelund, 1977). The correction factor for s_u proposed by Bjerrum (1973) is perhaps the most well-known way to account for rate effects (as well as anisotropy).

In conventional Finnish practice, s_u in clays is commonly determined using the field vane shear test. Recently, there have been indications in Finland that field vane shear test results may be yielding values of s_u that underestimate the true capacity of clay soils. This phenomenon has been attributed to problems with some of the coupling devices that are commonly used to measure shaft resistance when vane shear testing is performed without casing, which can lead to overestimation of the correction for shaft resistance. For Finnish railways, this behaviour has raised the concern that costly stability improvement actions are being performed in situations where they are unnecessary.

Manuscript received 6 June 2014; revised manuscript accepted 14 July 2015.
Discussion on this paper is welcomed by the editor.
* Department of Civil Engineering, Tampere University of Technology, Tampere, Finland.
† Department of Civil and Environmental Engineering, University of Delaware, Newark, DE, USA.

An alternative to the total stress analysis approach described above is the undrained effective stress analysis approach (e.g. Ladd, 1991). Following this methodology, effective stress shear strength parameters ϕ' and c' can reliably be determined from undisturbed samples in the laboratory. Assessments of field behaviour are then performed using effective stress shear strength analysis. The key challenge with this approach is how to assess the excess pore pressures that will be developed in the field as a result of the loads that are applied.

The amount of excess pore pressure that is developed in the field depends on the magnitude of the applied load, the properties of the clay and the rate of loading. It is well known that creep, or viscosity, has a large influence on soft clay behaviour (e.g. Arulanandan *et al.*, 1971; Augustesen *et al.*, 2004). In constant strain rate oedometer tests, higher loading rates result in higher stresses for the same amount of compression, which indicates that the preconsolidation pressure is rate dependent (e.g. Leroueil *et al.*, 1985; Augustesen *et al.*, 2004). Similar behaviour can also be observed in other types of tests that are performed to determine the shear strength of clay (e.g. Graham *et al.*, 1983; Leroueil *et al.*, 1985). Typically, higher loading rates yield higher undrained shear strength values, as shown in Fig. 1(a). The reason for this is that higher loading rates typically result in a smaller build-up of pore pressure, as illustrated in Fig. 1(b). Fig. 1(c) shows the corresponding effective stress paths. While the undrained shear strength increases with rate of loading, the effective strength parameters are generally not significantly influenced (e.g. Janbu & Senneset, 1995). Sheahan & Kaliakin (1999) suggest a 'correspondence principle' that states that rate-dependency, undrained creep effects and stress relaxation are all governed by the same basic mechanisms.

From a review of available literature on the behaviour of clay soils, the following conclusions can safely be drawn: (*a*) yielding of clays is time dependent, and (*b*) yield-induced pore pressure influences the undrained capacity of clays. While there are ample laboratory data on the time-dependent yield characteristics of clays, there seems to be very little field data available on this phenomenon. One real-world case

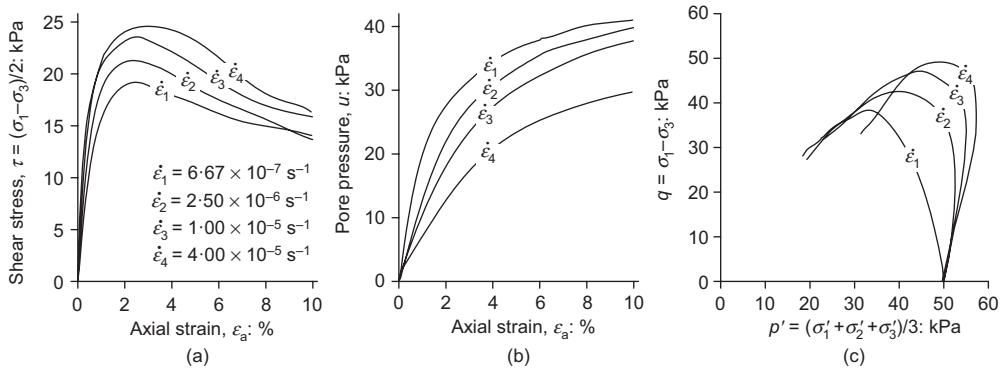

Fig. 1. Triaxial test results illustrating the effect of shear rate on: (a) shear stress; (b) excess pore pressure; (c) effective stress paths (data from Länsivaara (1996))

where rapid loading and subsequent undrained creep will have an effect on the stability of an embankment is a train coming to a standstill on a railway embankment constructed over a clay foundation. The occurrence of this loading condition is an issue of concern for the Finnish Transport Agency, as soft clay foundations underlie railway embankments at a significant number of locations throughout the Finnish rail network. This type of rapid loading represents a critical condition that must be assessed to ensure adequate stability at a given railway site. Even if an undrained stability failure does not occur immediately, stopped train loads that are sustained for any period of time also have the potential to induce undrained creep movements, potentially leading to undrained creep rupture. The use of distributed sensor networks to monitor impending stability problems or excessive creep movements is of particular interest to the Finnish Transport Agency, as part of assessing the on-going health of their rail network in real time.

As a result of a need for more field data in this area, this paper presents results from a full-scale failure load test that was conducted to evaluate the undrained loading capacity of a railway embankment on soft clay under rapid loading. The site was extensively instrumented, with a special emphasis on measuring excess pore pressure. The observations from this case history provide useful insight into the behaviour of embankments that fail by way of bearing capacity and global stability failure mechanisms.

FOUNDATION CONDITIONS AT THE EMBANKMENT TEST SITE

The embankment test site that is described in this paper is located on the south coast of Finland, near the town of Perniö. A non-operational railway track section that was built in the 1960s was utilised as the test site; this rail line is adjacent to the coastal railway track that connects Helsinki and Turku. An extensive soil investigation programme was performed to characterise the foundation conditions at this site, both prior to and following the failure experiment. The soil investigation in the immediate test area (Fig. 2) consisted of 25 soil borings performed with Swedish weight soundings (before the experiment), eight field vane shear test explorations, each with several vane shear test depths (before the experiment), and 19 cone penetration tests (CPTUs) with pore pressure measurements (ten before the experiment, nine after the experiment next to the pre-failure CPTU locations within the failure area). Before the experiment, disturbed soil samples were taken from three boreholes, and undisturbed samples from eight boreholes. Most of the undisturbed samples were taken using a Shelby tube-type piston sampler with a diameter of 50 mm, but Geonor-type piston samplers with 54 and 86 mm diameters were also used.

The general foundation stratigraphy in the load test area was determined using information obtained during the soil exploration process; a typical cross-section from the site is provided in Fig. 3. As shown, the soil layers at the site (from

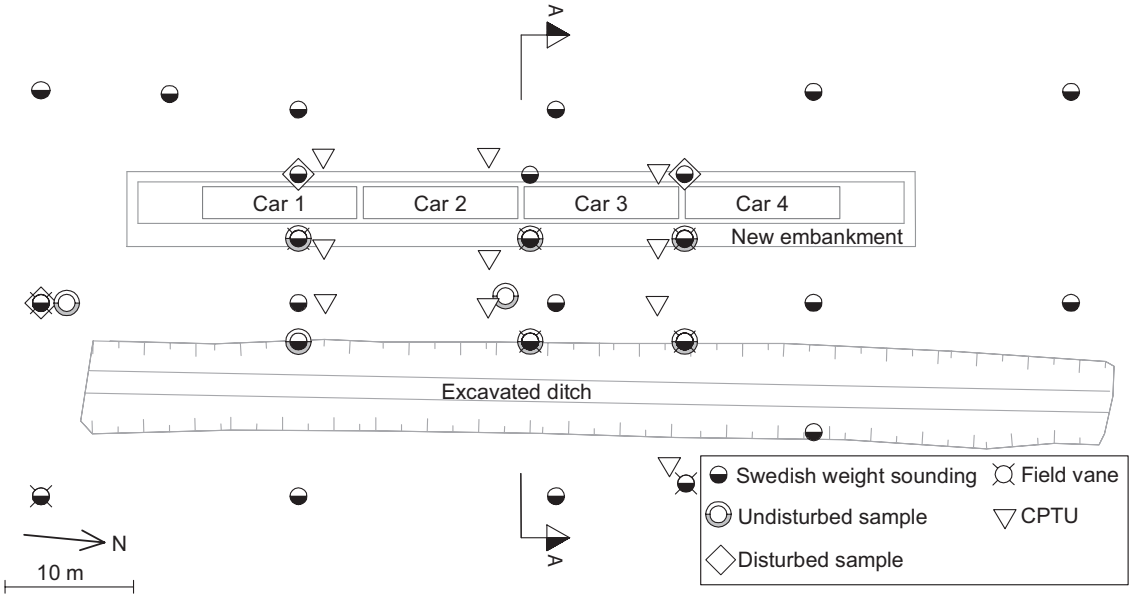

Fig. 2. Plan view of embankment test site showing location of soil borings and in situ tests

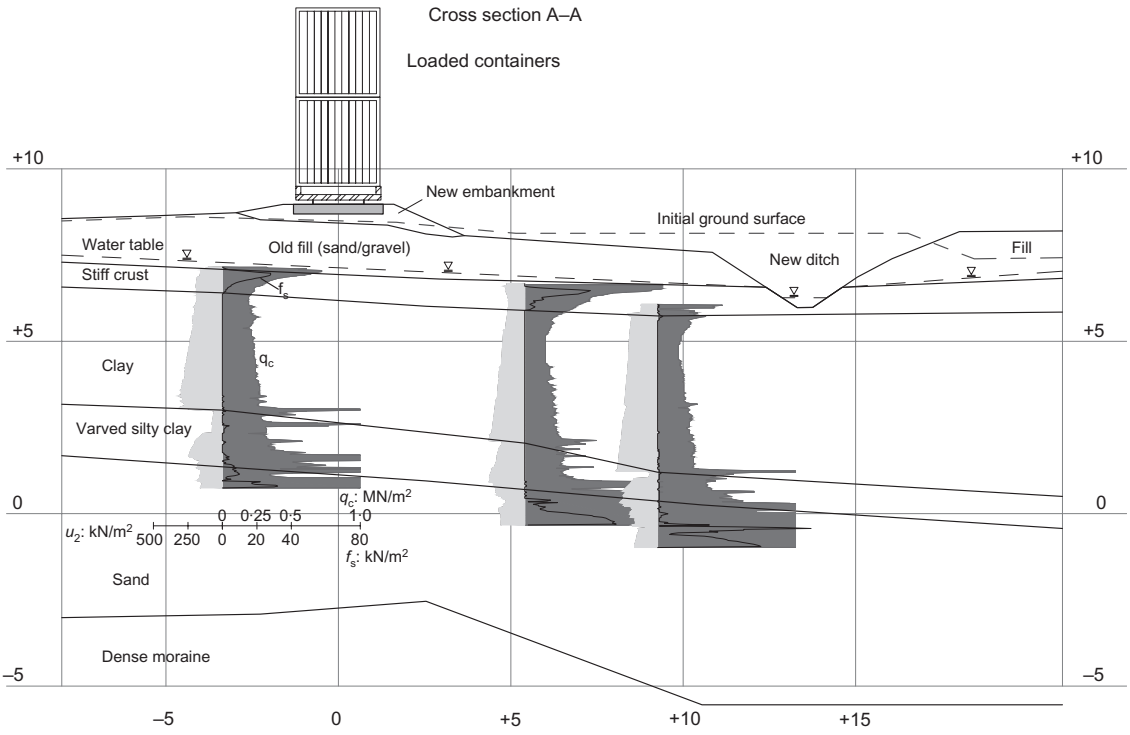

Fig. 3. Profile view of embankment test site showing soil stratigraphy inferred from the site investigation

top down) consist of: (*a*) an old fill made of sand and gravel with a thickness of about 1·5 m; (*b*) a 0·6–0·9 m thick weathered clay crust layer; (*c*) a 3·5–4·5 m thick soft clay layer; (*d*) a varved silty clay layer composed of thin clay, silt and sandy silt layers with a thickness of approximately 1·5 m (the overall classification for this layer according to EN ISO 14688-2 (SFS, 2005) is a sandy silty clay); (*e*) a significantly stronger sand layer with a thickness ranging from 2 to 6 m; and (*f*) a dense glacial moraine layer in which the soil explorations were terminated. The initial ground surface elevation across the site generally ranged from +7·5 m to +8·5 m above the Baltic Sea level. During the test the groundwater table was 1·3 m from the ground surface, which means that the stiff clay crust (which had likely previously been desiccated and above the groundwater table) was at an elevation below the groundwater level. At the beginning of the test, the pore water conditions at the site appeared to be hydrostatic. Fig. 4 shows the associated grain size analysis test results for the different soils that were present at the site, which were determined following SFS EN 933-1 (SFS, 2012), SFS EN 933-2 (SFS, 1996) and CEN ISO/TS 17892-4 (CEN, 2004a), as appropriate. The associated soil

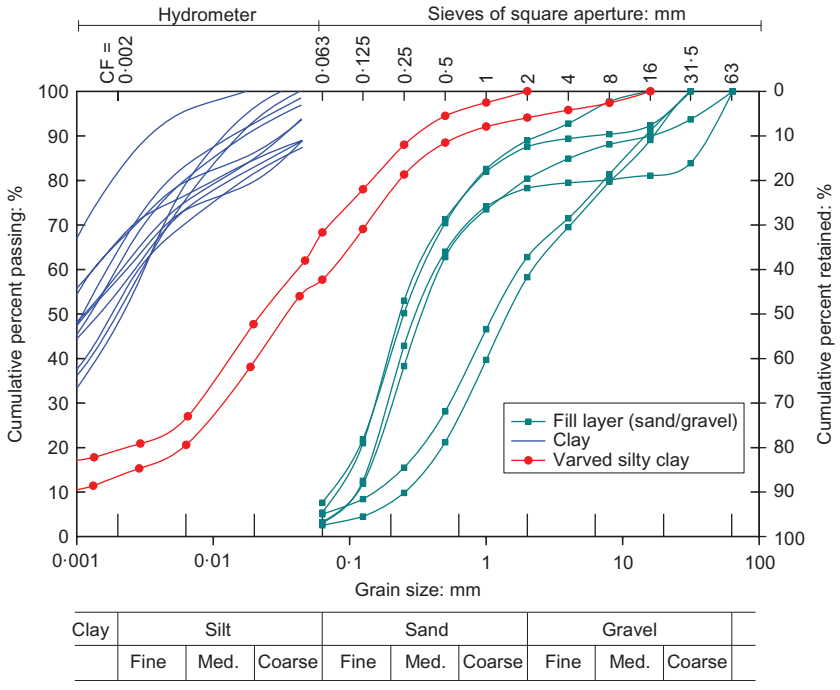

Fig. 4. Grain size analysis test results for Perniö soils

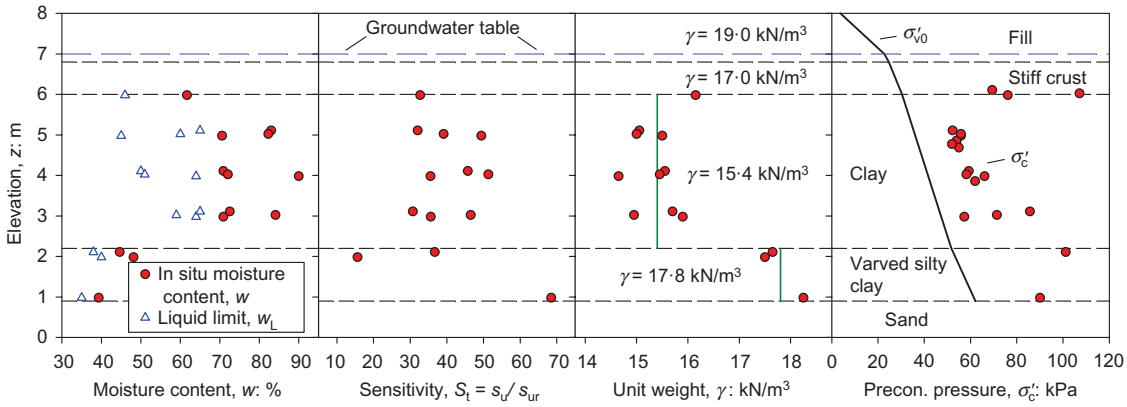

Fig. 5. General characteristics of Perniö clay, from samples taken at embankment toe

classifications for these soils were determined in accordance with SFS EN ISO 14688-2 (SFS, 2005).

From an embankment performance standpoint, the clay layer is of critical concern and was expected to govern the overall failure behaviour. Consequently, much of the field exploration programme and associated field test instrumentation were focused on characterisation and monitoring of this soil layer. Geologically, this soft clay layer is quite young; it was deposited after the last ice age, presumably some 8500 years ago, and it rose above the current sea level some 2000 to 3000 years ago due to post-glacial rebound (e.g. Soveri & Kauranne, 1976). The general characteristics of the clay are presented in Fig. 5. Data are shown for samples taken near the toe of the new embankment. The soil properties shown in this figure were determined using a series of fall cone tests (CEN ISO/TS 17892-6 (CEN, 2004b)) and constant rate of strain (CRS) consolidation tests (conducted at a loading rate of 0·6%/h, using the test equipment and procedure described by Kolisoja *et al*. (1987)).

As shown in Fig. 4, the clay content (<0·002 mm fraction) of the soft clay layer was in the range from 48 to 81%. Organic content tests (with heating to 800°C) on representative specimens yielded organic contents in the range from 0·1 to 1·0%. The measured unit weight of the soft clay ranged from 14·7 to 16·2 kN/m^3, with an average of 15·4 kN/m^3. Measured liquid limit values from the fall cone test had an average value of 57%. A few representative plastic limit tests (CEN ISO/TS 17892-12 (CEN, 2004c)) on samples collected slightly outside of the study area indicate that the plastic limit for this soil is generally in the range 29–36%. In situ water contents in the soft clay layer varied from 62 to 90%. These laboratory results yield plasticity index (PI) values in the range 36–49% and liquidity index (LI) values in the range 1·5–1·9. Historic leaching of salts from the clay structure by way of groundwater flow in the underlying coarser layers is possible but not confirmed.

An average sensitivity of 40 ($S_t = 40$) was determined using the fall cone test, which means that the remolded undrained strength of the clay is generally less than 0·5 kPa. From these properties (especially sensitivity, remolded strength and liquidity index), the clay may be classified as quick clay, depending on how one wishes to define it. The sensitivity and plasticity properties are also quite similar to some quick clays found in Sweden (Rankka *et al*., 2004).

As shown in Fig. 5, the clay is slightly overconsolidated. The largest overconsolidation ratio (OCR > 2) is found in the top portion of the clay layer. The viscosity or rate dependency of the clay given by the ratio C_α/C_c was in the range of 0·06 to 0·08, which is typical for similar Finnish inorganic clays.

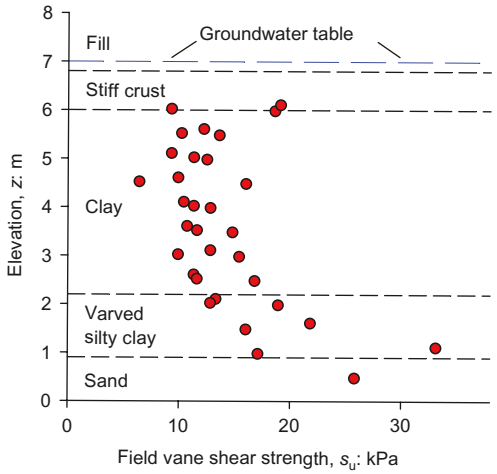

Fig. 6. Undrained strength characteristics of Perniö clay

Field vane shear test (in accordance with SGY (1999)) results from three combined soundings through the clay and varved silty clay layers are shown in Fig. 6. Near the top of the soft clay layer the minimum measured undrained shear strengths were in the range from 9 to 12 kPa and the average strength increase with depth was 1·15 kPa/m. A series of isotropically consolidated undrained shear triaxial compression tests were also performed, which indicated a peak friction angle of 25° for the soft clay.

TEST LAYOUT

As shown in Fig. 2 and Fig. 3, a new 0·6 m high railway embankment having a length of 60 m was constructed at the existing track location, 9 weeks prior to the load test. The reason for constructing this new embankment (or 'ballast layer') was that the old superstructure was deemed to be too weak to support the designed loading. The old wooden sleepers and light rails from the original track were also replaced with concrete sleepers and heavier rails. The side slopes of this embankment were generally 1:2. To reduce the overall stability at the site, 10 weeks before the experiment a 0·3 to 0·6 m layer of top soil was removed next to the embankment. Additionally, a 2 m deep ditch, 7 m wide, with a 1:1·5 side slope on the embankment side was excavated approximately 13·5 m from the embankment centreline (Fig. 3), to further reduce stability and to control the extents of the failure.

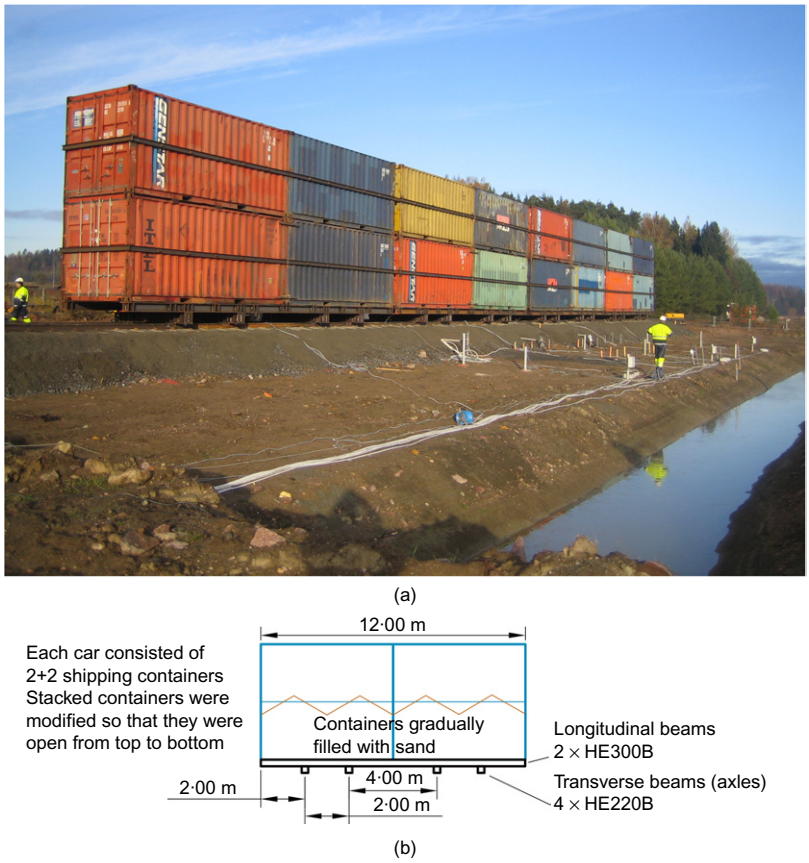

Fig. 7. (a) Test site and containers before loading; (b) container layout used to simulate train car loading pattern

A train coming to a standstill on the embankment was simulated by gradually filling modified shipping containers with sand. The containers rested on four steel frameworks that simulated four typical 12 m long two-bogey rail cars (Fig. 7). Each car had a stack of 2 + 2 containers. The tops of all containers and floors of the top containers were removed so as to be able to fill them without having to add the top row during the test. The frameworks distributed the load to the embankment by way of I-beams resting on the tracks. The beams were positioned so that they realistically matched a typical Finnish train axle configuration.

IN SITU INSTRUMENTATION

The two primary purposes of the in situ instrumentation were to collect data regarding the soil response during loading and failure, and to test the suitability of various in situ sensor systems for monitoring embankment stability

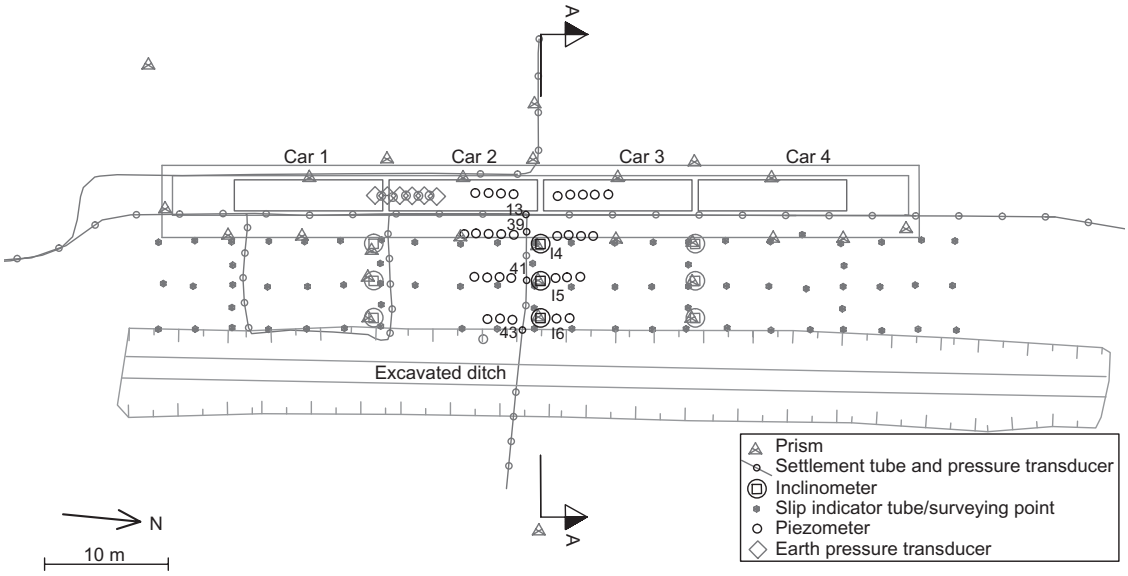

Fig. 8. In situ instrumentation layout at the Perniö test site. Piezometers, inclinometers and settlement transducers, the data from which are presented in Fig. 11, are shown using black symbols

under heavy train loading. The instrumentation was very extensive, with nearly 300 measurement points in the test area. Nearly all measurements were automated and constantly monitored during the experiment. A general map of the in situ instrumentation is provided in Fig. 8; this instrumentation is described below.

(*a*) Thirty-seven strain-gauge based piezometers were installed in a cross-section in the central part of the area. The piezometers used were foil-type units with a maximum pressure of 200 kPa. They were installed in the soft clay layer 3 weeks prior to the experiment by pushing them manually to the desired depth using an insertion rod. The intended function of the piezometers was to measure the yield-induced excess pore pressure close to failure at the slip surface. To be able to position the sensors in a useful manner, extensive pre-experiment stability analyses were carried out to predict the probable location of the failure zone. The piezometers were positioned in four groups: under the embankment centreline, under the embankment toe, halfway between the embankment and the ditch, and next to the ditch. In each group the piezometers were installed at 0·25 m depth intervals at the expected soil shear failure locations. The piezometers were installed with a 1 m horizontal spacing in the direction of the embankment so as to reduce the effects of soil disturbance. An additional deployment of five piezometers was utilised in a longitudinal pattern under the embankment centreline beneath the stiff clay crust layer to study the effect of non-uniform load distribution caused by the frameworks.

(*b*) Twenty-seven surveying prisms were positioned on the soil surface and the loading containers, which were monitored by two robotic total stations. The total stations were equipped with a monitoring routine that cycled through the prisms and also periodically checked for the orientation and location of the total stations themselves.

(*c*) Nine automatic two-axis inclinometers were installed in three cross-sections. Each 'in-place' inclinometer tube contained several inclination transducers at predetermined depths (0·5 m vertical spacing) that automatically logged the inclination profile of the tube at set time intervals.

(*d*) Three settlement tubes, with a total of 53 pressure transducers, were deployed throughout the test area. These custom-built automatic settlement tubes were developed at the soil and foundation structures laboratory at Tampere University of Technology (TUT). Each device consists of a flexible liquid-filled tube which contains pressure transducers at pre-determined locations. The tube is installed in the soil so that one end of the tube is fixed at a certain height level. When vertical displacements occur in the monitored area, the hydrostatic pressure acting on the transducers changes. The pressure changes are automatically recorded by the transducers, and the resulting data can be used to calculate the associated vertical displacements. Three tubes were used in the load test experiment (having lengths of 65 m, 70 m and 110 m) with 53 total transducers (six, 19 and 28 transducers in each tube, respectively).

(*e*) Five total stress earth pressure transducers were employed under the embankment. The vertical stress distribution under the train load was measured with five large-diameter ($D = 384$ mm), custom-built earth pressure transducers (manufactured at TUT) that were installed in the sand fill layer 1·5 m from the top of the embankment, along its centreline.

(*f*) Seventy-six slip indicators were used with surveying points on the surface, which were measured before and after the experiment. These in situ test devices consisted of flexible tubing that was installed vertically in the soil, which was used to determine the slip surface depth after the failure. Post failure, the depth of the slip surface was measured by lowering a 0·5 m long rod suspended on a cable down each tube until it could not advance any further. In addition, the surface ends of the tubes had surveying points installed. These points were surveyed before and after the experiment to map the ground surface movements in the test area.

(*g*) Thirty-two strain gauges were employed on the frameworks for weighing the containers. In order to accurately weigh the containers as they were loaded, the frameworks were equipped with strain gauges. The general effectiveness of this technique was confirmed by comparing the applied load measurements from the strain gauges against the known mass of the sand that was loaded onto the conveyor belt during the loading process.

TEST PROCEDURE AND OBSERVATIONS

Loading of the embankment began on 20 October 2009; the defined start time ($t = 0$) for the failure experiment was 15:30, and time stamps for various events during the load test are given as time elapsed (t = h:min) from this point. Loading was performed in increments using a telescopic conveyor belt. In each loading increment a load of 15 t was added to each car, corresponding to a 4·7 kPa train load increment. The applied load under each car is calculated using the following equation

$$q_{\text{app}} = \frac{W_{\text{sand}} + W_{\text{c}}}{L_{\text{c}} B_{\text{c}}} \tag{1}$$

where q_{app} = applied bearing pressure under a given car (kPa); W_{sand} = weight of sand loaded into a given car (kN); W_{c} = dead weight of the containers and framework of a given car, ca. 125 kN; L_{c} = length of car including spacing = 12·5 m; and B_{c} = width of the sleepers = 2·5 m.

For comparison purposes, the highest allowed axle load on the Finnish rail network is 25 t. For the four-axle 'cars' used in the experiment this corresponds to an applied bearing pressure of approximately 31 kPa. Fig. 9 shows the applied bearing pressure for each car over time during the Perniö load test. As shown, during the first 3 h of loading a train load of 24 kPa was applied on the two middle cars, and 21 kPa was

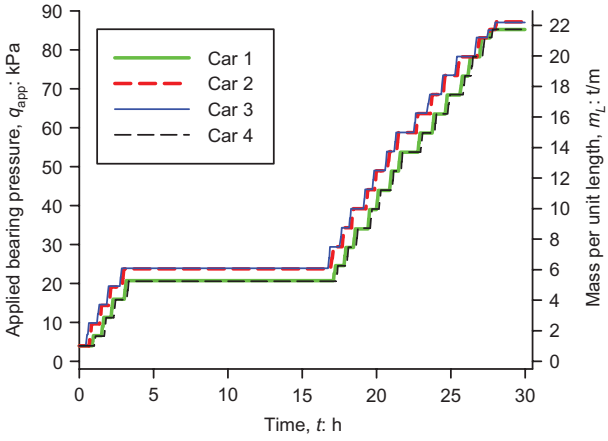

Fig. 9. Applied bearing pressure beneath each car over time during the Perniö load test

applied on the two outer cars. The load of the outer cars was intentionally kept slightly lower than the centre cars so as to trigger the eventual failure at the centre part of the area. The value of mass per unit length (m_L) shown on the right axis of this figure was obtained using the equation: $m_L = q_{app} \times B_c$. Although the loading in this figure is presented as uniform, it should be noted that in reality the load distribution in the soil varies slightly along the length of the embankment due to the realistic axle geometry of the cars.

The loading was halted at $t = 3{:}20$ for the night and continued in the morning of 21 October ($t = 16{:}45$). Throughout the loading process, gradual linear increases of displacements and pore pressures were recorded. The containers were loaded at an average rate of approximately 5·5 kPa/h until the loading was ended at $t = 28{:}04$. At this point, the centre containers had been completely filled to a load of 87 kPa (with the outer containers at 85 kPa). Under this constant load, displacements and pore pressures continued to increase. Accelerating pore pressure and displacement increases were recorded before failure. The first visual cues of an impending embankment failure were only minutes before failure when the cars began to tilt away from the instrumented side of the embankment. A total failure of the embankment occurred at $t = 29{:}57$, when the containers quickly sank and fell to their sides. Simultaneously, the soil next to the embankment moved upwards and laterally towards the ditch (Fig. 10).

Figure 11 provides some recorded observations of the failure behaviour of the Perniö railway embankment. Fig. 11(a) shows measured vertical and horizontal displacements and excess pore pressure from representative sensors from the middle of the test area (close to cross-section A–A). Fig. 11(b) shows the corresponding rates of change for the quantities presented in Fig. 11(a). The applied bearing pressure line (q_{app}) corresponds to the applied bearing pressure beneath car 2. The vertical displacement data (Δz) correspond to readings from representative settlement tube sensors at the embankment crest, embankment toe, halfway between the embankment and ditch, and at the edge of the ditch. The inclinometer data are the horizontal displacement (Δx) in three inclinometer tubes (I4, I5 and I6) at elevations +4·2 m, +4·0 m and +3·9 m, respectively. The chosen elevation level of approximately +4 m roughly corresponds to the level of highest displacement in tubes I4 and I5. The excess pore water pressure (Δu) data shown represent the average pore pressure values from groups of sensors (as discussed in more detail in the next section).

The data shown in Fig. 11(b) result from the differentiation of the data in Fig. 11(a); the raw differentiated data are smoothed with a simple exponential moving average filter (e.g. Holt, 2004) with a B value of 0·03. This large level of smoothing was required as the unsmoothed differentiated data are very noisy.

As shown in Fig. 11, yielding of the soil began at around $t = 26{:}40$; this start of yield is subject to interpretation, and appears a little more clearly in the Fig. 11(b) plots than in the Fig. 11(a) plots. As shown, loading was completed at $t = 28{:}04$, and failure of the embankment then occurred at $t = 29{:}57$. A more detailed discussion of the field measurements taken during the field test and after failure is provided in the following sections.

PORE PRESSURE RESPONSE DURING THE EMBANKMENT LOAD TEST

This section discusses the recorded pore pressure response. The following sensor behaviour groups were established based on location and qualitative pore pressure response (the average data from each of these groups are what is presented in Fig. 11)

- CL upper: under the embankment centreline, elevations +4·5 to +5·25 m (four piezometers)
- CL lower: under the embankment centreline, elevations +3·5 to +4·25 m (four piezometers)
- toe: under the embankment toe, elevations +2·25 to +4·25 m (eight piezometers)
- mid: midway between the embankment toe and the ditch, between elevations +2·5 to +4·0 m (seven piezometers)
- edge: next to the ditch, between elevations +3·25 and +4·5 m (four piezometers).

Clearly malfunctioning sensors (a total of four) were omitted from the data. For post-experiment analysis the piezometers under the embankment centreline were divided into two subgroups (i.e. CL upper and CL lower) owing to the distinctly different pore pressure response that was observed at different elevation levels (above or below +4·5 m).

Fig. 10. Post-failure photograph of the embankment failure area at the Perniö test site

During the initial loading (until $t = 26{:}00$ or so) a gradual and relatively linear increase of pore pressure was recorded by all piezometers. The general trend during loading was slightly accelerating (both against time and against external loading), as shown in Fig. 11. The effect of the loading steps can also be observed in the measured data, as shown in the pore pressure response plots in Fig. 11(b). The rate of pore pressure change during loading before $t = 26{:}00$ was around 1·5 to 2·0 kPa/h under the embankment (for comparison purposes, recall that the average rate of loading was approximately 5·5 kPa/h). It is likely that during this phase of load application the stiff clay crust carried a significant portion of the applied load, which resulted in a fairly stiff overall response of the embankment foundation.

A qualitative change in the pore pressure response began to emerge in the very late stages of loading. At $t = 25{:}35$ (corresponding to a 78 kPa train load in the centre cars), piezometers from group CL upper began to indicate an accelerating pore pressure response that was notably higher than the response from previous similar loading steps.

At approximately $t = 26{:}00$ (78 kPa train load) sensors from group CL lower (the lower sensors under the embankment centreline) began to indicate deceleration, eventually turning to a decrease of pore pressure after $t = 27{:}25$. The most likely reason for this is that the soil mass above these units had moved enough to slightly pull the piezometers by their wiring. This would cause a pressure decrease near the tips of the piezometers where the porous stone was located.

At $t = 26{:}40$ (an approximate train load of 83 kPa) piezometers in groups CL upper, toe and mid simultaneously began to indicate a continually accelerating increase in pore pressure that continued uninterrupted until failure. The group edge, which was farthest away from the embankment, also exhibited accelerating pore pressure changes after $t = 26{:}40$, but the trend in changing pore pressure values was less pronounced than what was observed with the other piezometer groups. The brief decrease of pore pressure recorded by group CL lower was sharply reversed after $t = 27{:}40$.

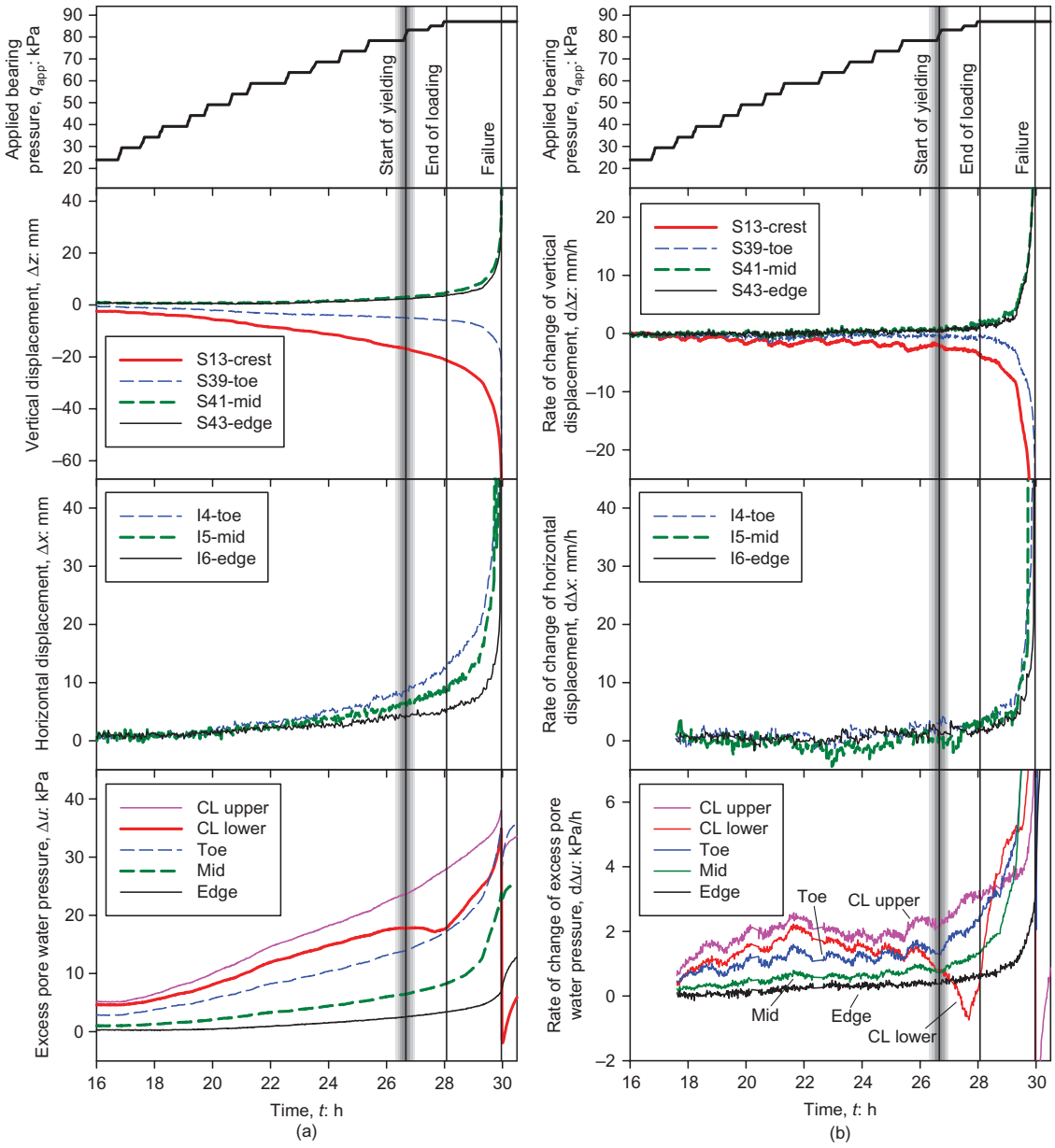

Fig. 11. Observed failure behaviour of the Perniö railway embankment: (a) loading, displacements and excess pore water pressure with time; (b) corresponding time differentials (rates of change) with time

Loading was ended at $t = 28{:}04$, with the load in the centre cars being held constant at 87 kPa. This had no visible effect on the already accelerating trend of pore pressure increase.

More drastic accelerations of pore pressure increase were recorded in the toe and mid groups at $t = 28{:}40$, and the edge group at $t = 29{:}20$. Groups CL upper and CL lower exhibited similar 'final accelerations' at $t = 29{:}30$ (exact times are subject to interpretation). The authors speculate that these final accelerations in pore pressure response may have been to some extent caused by the total failure of the stiff clay crust layer, which would have further increased the load acting on the soft clay layer.

Figure 12 shows the profile of excess pore pressure in the centre cross-section A–A at $t = 28{:}00$ (end of loading), at $t = 29{:}30$ (ca. 28 min before failure) and right before final failure. The contours are interpolated between individual readings (with the results from malfunctioning sensors omitted). The general shape of the slip surface and its progression with time at constant loading can be observed in the pore pressure contours.

Failure occurred at $t = 29{:}58$. Table 1 shows the measured highest and average Δu values before failure ($t = 29{:}57$), and the average Δu values immediately after failure ($t = 29{:}59$) for each piezometer group.

At failure, sensors in the CL lower group instantaneously exhibited a very large drop in pore pressure, with many even indicating suction. Groups CL upper, toe and mid also indicated slight drops in pore pressure at failure, but their magnitudes were quite small compared to the CL lower group. The measured drops in all cases were very temporary, as the pore pressure quickly began to increase again. This post-failure increase lasted for approximately 50–65 h before approaching steady values. Pore pressure measurements were continued for 8 days after the experiment. During this time the measured pore pressures remained at a high level, with a slightly decreasing trend.

A likely explanation for the sharp drop in pressure that was observed in the CL lower group readings is that the piezometers were rapidly pulled out from their positions at failure (i.e. similar behaviour as what was observed with the CL lower sensors after $t = 27{:}25$). The subsequent fast increase in pore pressure after failure would indicate local equilibration of pore pressure around the sensor after its pullout. It is likely that the piezometers indicating a large drop in pore pressure (i.e. the CL lower group) were outside the final failure surface.

DISPLACEMENT RESPONSE DURING THE EMBANKMENT LOAD TEST

A response similar to what was observed with the pore pressure measurements was also observed with the horizontal and vertical displacement monitoring systems. As shown in Fig. 11, the vertical and horizontal displacement responses during initial loading exhibited a fairly flat slope, with any changes in slope reasonably being attributed to the corresponding increase in load that was being applied. As noted previously, some observed changes in pore pressure behaviour began to occur around 26:40; after this point, more significant changes were generally observed to occur in most sensors. Associated horizontal movements during the

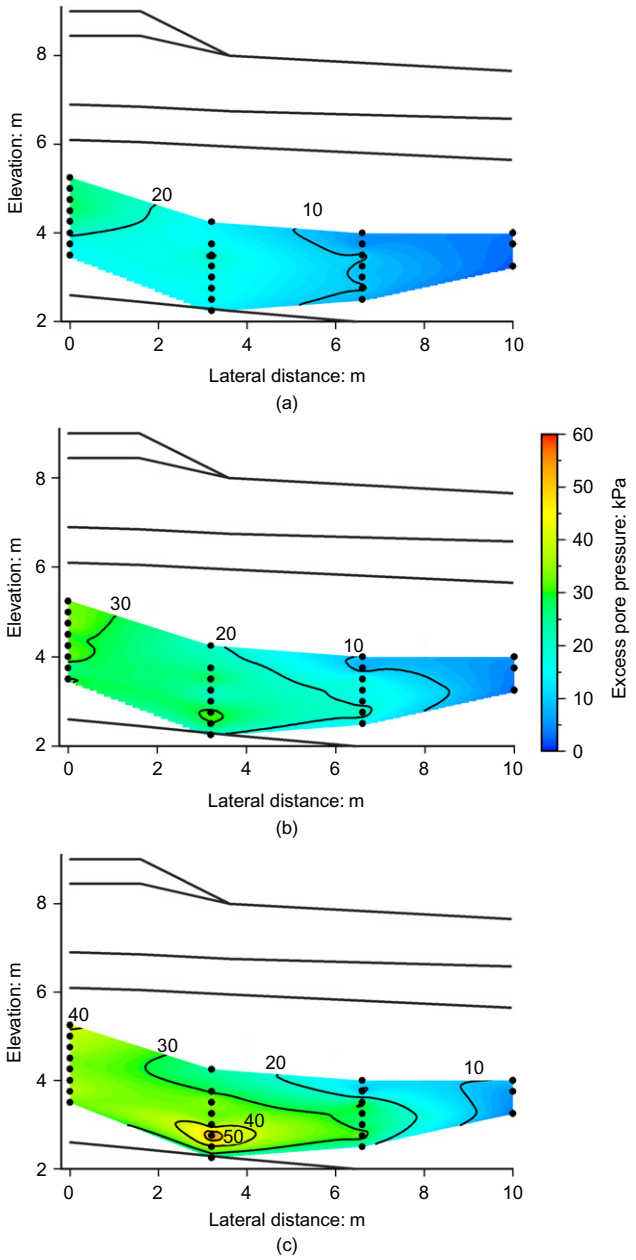

Fig. 12. Excess pore pressure profile inferred from piezometer measurements along cross-section A–A, at: (a) $t = 28{:}00$; (b) $t = 29{:}30$; (c) $t = 29{:}57$. The full load has been applied at all stages. Piezometer locations are shown

Table 1. Measured Δu values before and after failure

Pore pressure sensor group	Highest Δu value before failure ($t = 29{:}57$) and the average sensor elevation level	Average Δu value before failure ($t = 29{:}57$): kPa	Average Δu value immediately after failure ($t = 29{:}59$): kPa
CL upper	41·2 kPa; +5·25 m	37·9	30·5
CL lower	38·3 kPa; +3·75 m	33·9	−1·3
Toe	59·4 kPa; +2·75 m	35·0	27·8
Mid	32·9 kPa; +2·75 m	23·2	22·2
Edge	9·2 kPa; +4·0 m	7·1	7·4

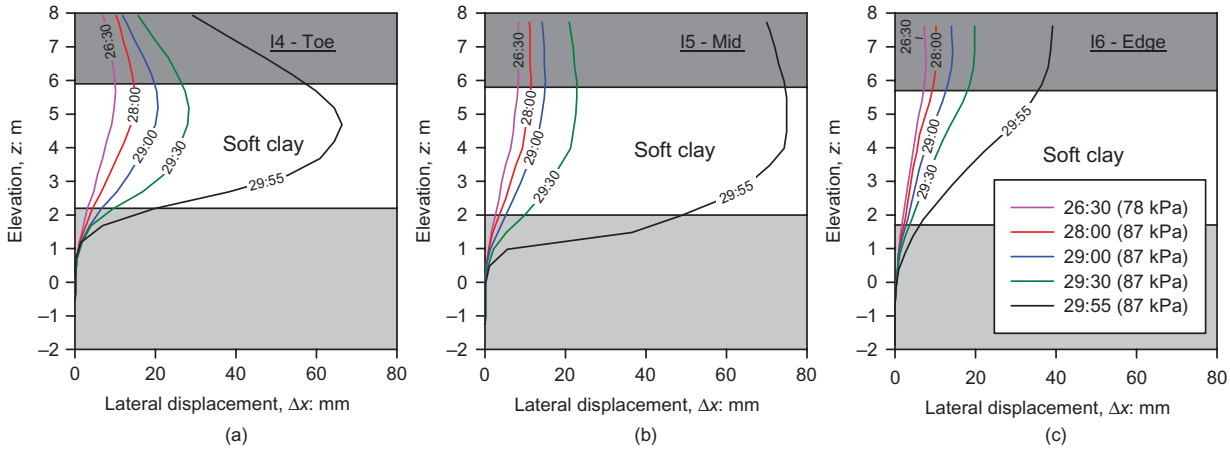

Fig. 13. Horizontal displacement measurements in the foundation: (a) at embankment toe; (b) at midpoint between embankment and ditch; (c) at edge of ditch

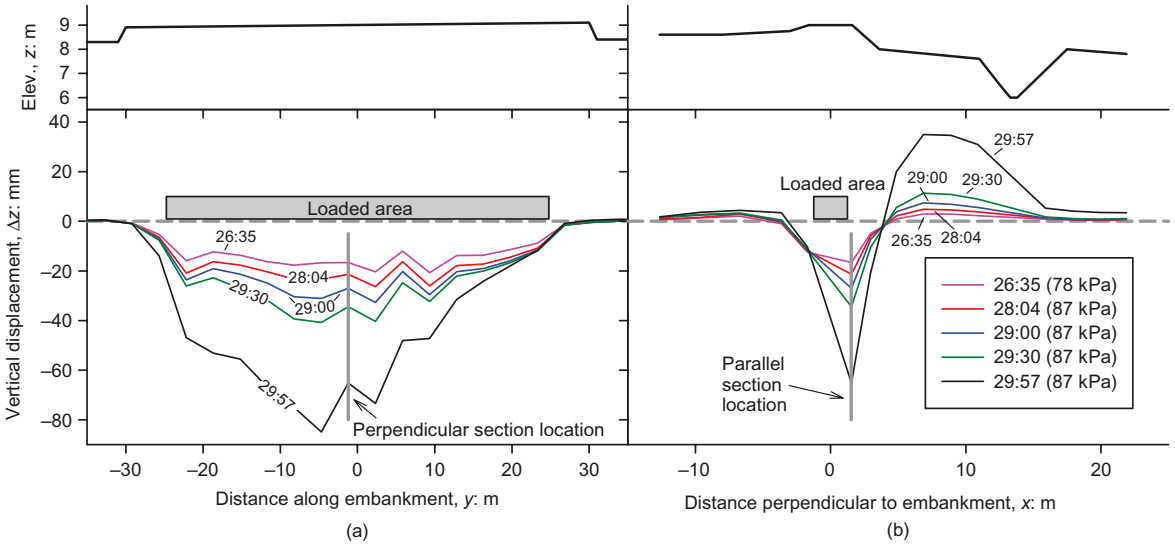

Fig. 14. Vertical displacement measurements at the ground surface: (a) along embankment crest; (b) perpendicular to embankment along section A–A

yielding process that were recorded in the foundation soil by inclinometers at the toe, mid and edge locations are provided in Fig. 13. Fig. 14 shows the vertical displacement measurements that were recorded by settlement tubes at the ground surface during the same time frame, along the embankment crest and perpendicular to the embankment along section A–A.

As shown in Fig. 11, Fig. 13 and Fig. 14, horizontal and vertical displacements continued to occur at a constant load level (87 kPa) past $t = 28{:}00$, increasing at an accelerating rate until failure. Data from inclinometers and total station measurements indicated that during loading and prior to failure the soil mass between the embankment and the ditch moved so that lateral displacements on the ground surface (not shown here) were fairly uniform regardless of the distance from the embankment.

As shown in Fig. 13, the horizontal displacements that occurred were dominated by movement in the soft clay layer. Some significant movements were also observed in the underlying stratified silty clay layer, especially at the midpoint location (i.e. inclinometer I5). It is hypothesised that a significant amount of the observed displacements in the silty clay layer may have been caused by inclinometer tube movements in the soft clay layer, which dragged the underlying tube section along in the somewhat stiffer layer. This hypothesis is supported by other field measurements and analyses.

The vertical displacement response along the embankment centreline exhibited a fairly uniform and consistent trend (Fig. 14(a)), yielding a 'bowl-shaped' depression as movement occurred. Perpendicular to the embankment, the magnitude and direction of the measured vertical displacements were highly dependent on the distance from the embankment (Fig. 14(b)). The embankment exhibited displacement downwards under the load area, while a significant portion of the area between the embankment and the ditch moved upwards. The largest pre-failure settlements (−85 mm) were observed at the embankment crest close to the centre cross-section (Fig. 14(a)). The largest upward displacements (+35 mm) occurred close to halfway between the embankment and the ditch, approximately 7 m away from the embankment centreline (Fig. 14(b)). At the embankment toe vertical displacements were very small, which is a result of the particular failure geometry that occurred.

POST-FAILURE DISPLACEMENTS

Figure 15 shows the final horizontal displacement vectors that were recorded from the ground surface surveying points.

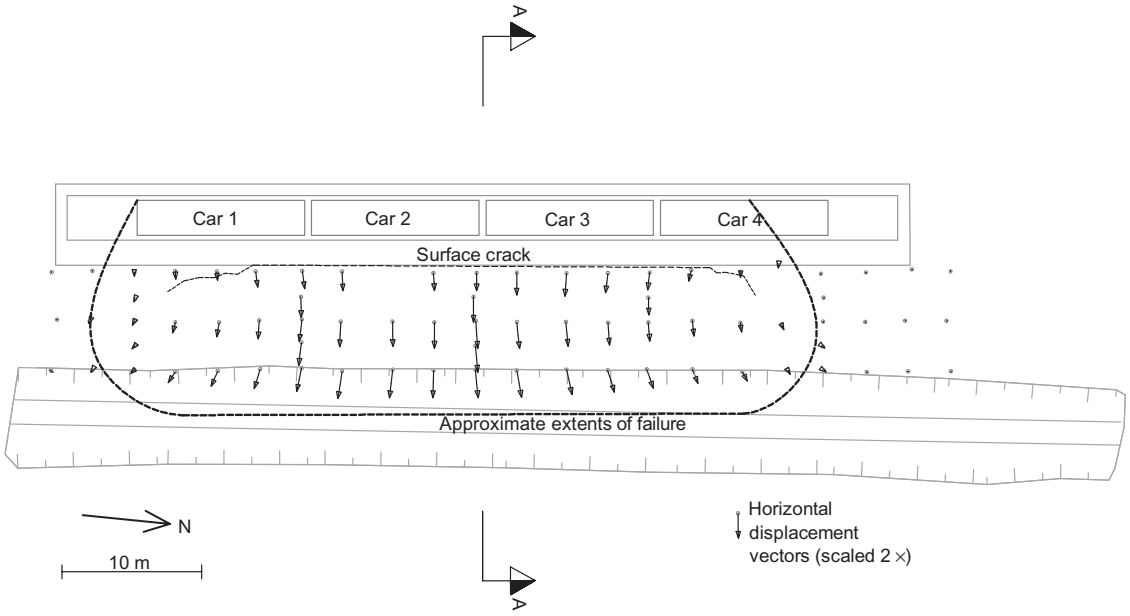

Fig. 15. Measured horizontal displacement vectors at ground surface from the beginning to the end of the experiment, at the various survey point locations. Also shown are approximate extents of failure and a surface crack that opened up at failure

As shown, the failure was confined between the embankment and the ditch, with practically no displacements being observed beyond the ditch. The width of the failure area was approximately 50 m, roughly the loaded length of the embankment. Owing to a locally stiffer and thinner layer of soft clay, the displacements near car 4 were slightly smaller than those at the other end of the loaded area (car 1).

The largest measured ground surface deformations post-failure occurred under car 2, and were generally consistent with the observed pre-failure deformation pattern. The largest measured embankment settlement after failure was −1·07 m, the largest heave was +0·70 m (at 10·9 m from the centreline of the embankment), and the largest lateral surface movement was 0·98 m. It should be noted that the largest embankment settlement was likely more than the value measured by the settlement tubes, but for safety reasons it could not be confirmed by other more direct means.

After the total failure of the embankment, no further soil movements outside the limits of measurement accuracy were recorded with any of the monitoring systems. This indicates that the soil mass reached its new equilibrium practically instantaneously at failure.

SLIP SURFACE AND FAILURE MECHANISM

Post-failure measurements of the slip surface location remained generally inconclusive. At failure the inclinometer tubes had moved with and in relation to the soil mass at failure. Some tubes were also dislodged from their bottom anchor point at failure. Thus the post-failure locations of the inclinometers' measurement points were unclear. The slip indicator tubes also proved inconclusive. The tubes had significant bending above the actual shear zone, and in most cases the 500 mm steel rod used for probing was stopped very close to the surface due to the large displacements that had occurred.

The best information on the shape of the failure surface comes from the pre-failure pore pressure readings, coupled with general observations from the inclinometer readings. Fig. 16 shows the 'best guess' failure surface location that was determined by analysis of the different sensors. In general, observations indicate a zone of high shear deformations in the soft clay layer rather than formation of a distinct slip surface, so the discrete failure surface that is shown could also perhaps be expressed as a zone of general plastic shear deformation of varying magnitude (Fig. 16). As shown, the inferred shear zone extended from behind the railway sleepers to the lower level of the soft clay layer under the embankment toe. From there it gradually curved back up, ending at the bottom of the ditch. Observed inclinometer movements in the varved silty clay layer that underlies the soft clay layer are largely attributed to dislodgement and dragging of the lower portions of the inclinometer casing as a result of the large strains that occurred in the soft clay layer.

The field data and associated observations point to a bearing capacity type failure. The failure mechanism likely contained an active zone beneath the loaded area that moved down and outward, a direct shear zone under the embankment toe, and a passive zone that moved upwards and outwards towards the ditch (Fig. 16). At failure a distinct crack (with a width up to 0·5 m) opened on the soil surface at the embankment toe. It is believed that this crack extended to the bottom of the fill layer.

DISCUSSION

A noteworthy finding from this study is that a significant change in the pore pressure and displacement response occurred only at a very late stage in the experiment. The highest rates of change in both pore pressures and displacements were measured only after loading ended, during the time period when the rapidly applied load was kept constant. The likely reason for this behaviour lies in the time- and rate-dependent behaviour of the soft clay layer. The described behaviour points to an undrained creep rupture caused by the constant external load.

Following the hypothesised mechanism of failure, the deviator stress in the clay beneath the embankment was raised to a high level close to failure due to the applied load. Under this condition, the resulting shear-induced excess pore pressure is partly governed by the viscous properties of the clay, that is, creep. Under a constant load, measured pore pressures increased at an accelerating rate until failure. In this sense, the experiment is analogous to an undrained creep test

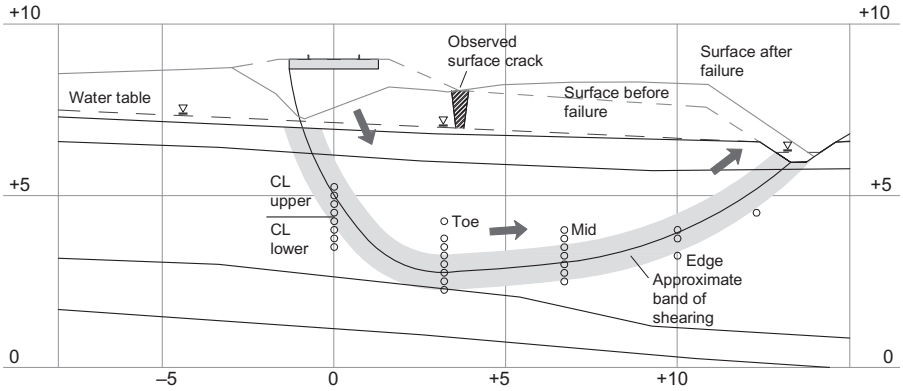

Fig. 16. Hypothesised failure surface location and general band of shearing based on overall analysis of field sensor data. Piezometer locations are shown

that leads to failure at a sufficiently high deviator stress (e.g. Sheahan, 1995). During undrained shear, lightly overconsolidated clay tends to contract, which causes an increase in pore pressure such that a constant volume condition is maintained. This response is dependent (among other things) on the loading rate, or the time a constant load increment is sustained.

For the field study described here, it is likely that the onset of failure was fairly localised, with failure first occurring somewhere close to the embankment, followed by progressive failure throughout the shear band. Given the nature of the recorded data, it is difficult to find clear indicators of failure progression from one location to another. It is quite possible that the observed time-dependency of the pore pressure response is due in part to progressive development of the shear band and associated localised shear stress/strain concentrations. Over time, as the shear band formed, pore pressures would have increased accordingly along the entire slip surface.

The highest pore pressure at failure was measured at the toe of the embankment (Fig. 12). This pore pressure concentration may be due to the proposed sliding mechanism (Fig. 16) where a downward-moving 'active' soil block may have transitioned into a more horizontally displacing sliding mass, causing large strains and stress concentrations.

Overall, it is believed that the failure occurred under 'true' undrained conditions due to the relatively low permeability of the foundation soils involved, and the short duration of loading prior to failure. Given these constraints, it is expected that pore water migration would have occurred only over a relatively thin zone of soil that was adjacent to one of the more permeable boundaries.

This proposed mechanism of failure is generally consistent with what has been noted by others (e.g. Arulanandan *et al*., 1971; Holzer *et al*., 1973), who observe that once a certain threshold level of deviator stress is reached, subsequent undrained creep will lead to a continually increasing rate of strain and pore pressure increase, eventually leading to failure. Higher deviator stress levels lead to a reduced time to failure and vice versa. Below a threshold level of deviator stress, undrained creep will not cause the soil to fail, with the soil instead reaching a certain constant equilibrium stress state below the failure envelope.

Thinking back to the general 'stopping train' problem that this load test was designed to simulate, there is thus no single failure load value that can be determined without taking time into account. Instead, failure for a given set of soil conditions is governed by both the magnitude of the applied load (i.e. the applied deviator stress), and the time over which that load will be sustained. Possible stress paths to failure under the embankment, with loading corresponding to different deviator stress levels, are shown in Fig. 17.

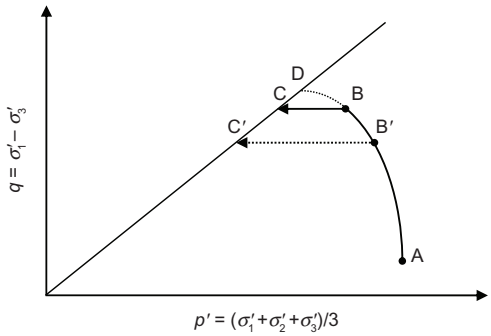

Fig. 17. Conceptual example of hypothesised effective stress paths under embankment. ABC: Stress path in the test. ABD: Possible stress path if loading had been continued further (less time to failure, less shear-induced pore pressure Δu_s). AB′C′: Possible stress path if loading had been stopped earlier (more time to failure, more Δu_s)

Following these observations, for a given 'stopped train' problem, it should be possible to determine a safe load level that will not cause failure after any amount of time. This condition would correspond to a shear stress level that is low enough not to lead to a creep failure of the soil. One such approach that may be useful in this regard has been proposed by Sheahan (1995), who suggested that a 'static yield surface' be determined by a series of undrained triaxial creep tests or sufficiently slow CRS triaxial tests.

The issue of ultimate bearing capacity of the Perniö loading test has also been researched by Mansikkamäki (2015), who used advanced elasto-viscoplastic soil models that account for soil creep. According to these studies, a 70–80 kPa load would have been sufficiently large enough to cause a creep failure if it was sustained for a long enough duration.

It appears likely that the stiff clay crust had a large distributing effect on the applied load during initial loading, which would explain the initially stiff response of the foundation soils. The sudden changes in pore pressure and displacement that occurred in the final stages of the test could have been partly caused by a general failure of the stiff clay crust layer.

The best indicators for an impending failure seem to have been the excess pore pressure response under the embankment toe, the embankment settlement and lateral movements in the soil. The rates of change in the pore pressure response ($d\Delta u/dt$) or displacement (ds/dt) appear to be more reliable safety

indicators than the measured absolute values themselves. Had the case been a real-life embankment under monitoring, any clear alarm limits would have been very difficult to determine in real time owing to large variation in the measured variables.

The present authors' experience with this project has indicated that the proper positioning of monitoring equipment is a case-sensitive issue and should be based on sufficient stability analyses that identify the most probable failure mechanisms. With regards to monitoring of similar in-service train embankments, proper placement of instruments according to predicted failure mechanisms is consequently clearly important.

CONCLUSIONS

A small railway embankment on soft clay subsoil was brought to failure with rapid loading, simulating a train coming to a standstill. The embankment was loaded with a 'train-sized' finite area surcharge that was increased up to 87 kPa, over the course of 28 h. The embankment failed at $t = 29{:}57$ from the start of the experiment, under a steady sustained surcharge of 87 kPa. The observed shear geometry indicated an asymmetric bearing capacity mechanism of failure. The failure was evidently triggered by an undrained creep rupture.

The main conclusions from this failure experiment are given below.

(*a*) A review of previous literature indicates that the pore pressure and deformation response of soft clay under undrained loading is highly time and rate dependent. Similar behaviour was observed in the current failure experiment, in which undrained creep rupture seems to have been the governing mode of failure.

(*b*) Owing to conclusion (*a*), the ultimate bearing capacity of an embankment on soft clay subjected to a rapidly applied and subsequently sustained loading (e.g. a train coming to a standstill) is governed both by the magnitude and the duration of loading.

(*c*) Because of conclusion (*b*), the stability design of such embankments should in principle take into account the duration for which high load levels are sustained. A review of available literature indicates that it may be possible to determine a safe load level that is small enough not to cause an undrained creep rupture, even for loads that are sustained for a very long period of time.

(*d*) Sudden changes in the rates of deformation and pore pressure increase close to the embankment are the best indicators of an impending failure. The proper placement of monitoring instruments should be performed based on predictions of the likely failure mechanisms for a given geometry.

This field test provides valuable input in relation to developing methods for undrained stability analysis. These analyses will be presented in a separate paper. The various degrees of usefulness for the measurements that were made provide valuable information for others that are seeking to design an 'early warning system' or a 'structural health monitoring system' for railway embankments constructed on soft clay foundations.

AVAILABILITY OF DATA

The authors together with the Finnish Transport Agency have decided to make the full experimental data available for all those interested. The data can be accessed from: http://urn.fi/urn:nbn:fi:csc-kata20150507094517328502

ACKNOWLEDGEMENTS

The authors would like to thank the Finnish Transport Agency for making the project possible with their generous funding and support, as well as everyone involved in preparing and conducting the experiment. Professor Meehan would like to acknowledge the support of the Fulbright Center in Finland and the 2012–2013 Fulbright-Tampere University of Technology Scholar Award, which provided support for work on this manuscript.

NOTATION

B	width (m)
C_c	compression index
C_α	secondary compression index
c'	cohesion (kPa)
L	length (m)
m_L	mass per unit length (tonne/m)
q_{app}	applied bearing pressure (kPa)
S_t	sensitivity
s_u	undrained shear strength (kPa)
s_{ur}	remoulded undrained shear strength (kPa)
t	elapsed time (h)
u	pore pressure (kPa)
W	weight (kN)
w	water content (%)
w_L	liquid limit (%)
z	elevation from sea level (m)
γ	unit weight (kN/m^3)
ε_a	axial strain (%)
σ_c'	preconsolidation stress (kPa)
σ_{v0}'	vertical effective stress (kPa)
ϕ'	friction angle (degrees)

REFERENCES

Arulanandan, K., Shen, C. & Young, R. (1971). Undrained creep behaviour of a coastal organic silty clay. *Géotechnique* **21**, No. 4, 359–375, http://dx.doi.org/10.1680/geot.1971.21.4.359.

Augustesen, A., Liingaard, M. & Lade, P. V. (2004). Evaluation of time-dependent behavior of soils. *Int. J. Geomech.* **4**, No. 3, 137–156.

Bjerrum, L. (1973). Problems of soil mechanics and construction on soft clays and structurally unstable soils (collapsible, expansive and others). *Proceedings of the 8th European conference on soil mechanics and foundation engineering*, Moscow, vol. 3, pp. 111–159.

CEN (European Committee for Standardisation) (2004a) ISO/TS 17892-4: Geotechnical investigation and testing. Laboratory testing of soil. Part 4: Determination of particle size distribution. Brussels, Belgium: CEN.

CEN (2004b) ISO/TS 17892-6: Geotechnical investigation and testing. Laboratory testing of soil. Part 6: Fall cone test. Brussels, Belgium: CEN.

CEN (2004c) ISO/TS 17892-12: Geotechnical investigation and testing. Laboratory testing of soil. Part 12: Determination of Atterberg limits. Brussels, Belgium: CEN.

Graham, J., Crooks, J. & Bell, A. (1983). Time effects on the stress–strain behaviour of natural soft clays. *Géotechnique* **33**, No. 3, 327–340, http://dx.doi.org/10.1680/geot.1983.33.3.327.

Helenelund, K. V. (1977). *Methods for reducing undrained shear strength of soft clay*, report no. 3. Linköping, Sweden: Swedish Geotechnical Institute.

Holt, C. C. (2004). Forecasting seasonals and trends by exponentially weighted moving averages. *Int. J. Forecasting* **20**, No. 1, 5–10.

Holzer, T. L., Höeg, K. & Arulanandan, K. (1973). Excess pore pressures during undrained clay creep. *Can. Geotech. J.* **10**, No. 1, 12–24.

Janbu, N. & Senneset, K. (1995). Soil parameters determined by triaxial testing. *Proceedings of the 11th European conference on soil mechanics and foundation engineering*, Copenhagen, vol. 3, pp. 101–106.

Kolisoja, P., Sahi, K. & Hartikainen, J. (1987). Automated oedometer device. *Proceedings of the 9th European conference on soil mechanics and foundation engineering*, New Delhi, vol. 1, 39–42.

Ladd, C. C. (1991). Stability evaluation during staged construction. *J. Geotech. Engng* **117**, No. 4, 540–615.

Länsivaara, T. (1996). *Maan mekaanisen käyttäytymisen mallintaminen*. Licensiate thesis, Tampere University of Technology, Tampere, Finland (in Finnish, English title 'Modelling the mechanical behaviour of soil').

Leroueil, S. & Soares Marques, M. E. (1996). Importance of strain rate and temperature effects in geotechnical engineering. In *Measuring and modeling time dependent soil behavior* (eds T. C. Sheahan and V. N. Kaliakin), Geotechnical Special Publication no. 61, pp. 1–60. New York, NY, USA: American Society of Civil Engineers (ASCE).

Leroueil, S., Kabbaj, M., Tavenas, F. & Bouchard, R. (1985). Stress–strain–strain rate relation for the compressibility of sensitive natural clays. *Géotechnique* **35**, No. 2, 159–180, http://dx.doi.org/10.1680/geot.1985.35.2.159.

Mansikkamäki, J. (2015) *Effective stress finite element stability analysis of an old railway embankment on soft clay.* Doctoral thesis, Tampere University of Technology, Tampere, Finland.

Rankka, K., Andersson-Sköld, Y., Hultén, C., Larsson, R., Leroux, V. & Dahlin, T. (2004). *Quick clay in Sweden*, report 65, 145. Linköping, Sweden: Swedish Geotechnical Institute.

SFS (Finnish Standards Association) (1996) SFS EN 933-2: Tests for geometrical properties of aggregates. Part 2: determination of Particle size distribution. Test sieves, nominal size of apertures. Helsinki, Finland: SFS.

SFS (2005) SFS EN ISO 14688-2: Geotechnical investigation and testing. Identification and classification of soil. Part 2: Principles for a classification. Helsinki, Finland: SFS.

SFS (2012) SFS EN 933-1: Tests for geometrical properties of aggregates. Part 1: determination of particle size distribution. Sieving method. Helsinki, Finland: SFS.

SGY (Suomen Geoteknillinen Yhdistys (Finnish Geotechnical Society) (1999). *Kairausopas II, Siipikairaus.* Nummela, Finland: Finnish Geotechnical Society (in Finnish, English title 'Soil boring manual II, Vane shear test').

Sheahan, T. C. (1995). Interpretation of undrained creep tests in terms of effective stresses. *Can. Geotech. J.*, **32**, No. 2, 373–379.

Sheahan, T. C. & Kaliakin, V. N. (1999). Microstructural considerations and validity of the correspondence principle for cohesive soils. In *Proceedings of the 13th conference on engineering mechanics*, Baltimore, MD, USA (eds N. Jones and R. Ghanem). Reston, VA, USA: American Society of Civil Engineers (ASCE).

Soveri, U. & Kauranne, L. K. (1976). *Rakennusgeologia I, Suomen rakennusgeologia*. Espoo, Finland: Otakustantamo (in Finnish, English title 'Civil engineering geology I, Finnish civil engineering geology').